The Crop Journal 14 (2026) 107–116

Contents lists available at ScienceDirect

The Crop Journal

journal homepage: www.keaipublishing.com/en/journals/the-crop-journal/

A synthetic glycolate metabolism bypass in rice chloroplasts increases photosynthesis and yield

Xiangze Chen [a], Guangru Li [a], Haohui He [a], Wenle Xie [a], Lili Cui [b], Zhisheng Zhang [a,c], Xinxiang Peng [a,c], Guohui Zhu [a,c,*]

[a] Guangdong Provincial Key Laboratory for the Development Biology and Environmental Adaptation of Agricultural Organisms, College of Life Sciences, South China Agricultural University, Guangzhou 510642, Guangdong, China
[b] Rice Research Institute, Fujian Academy of Agricultural Sciences, Fuzhou 350019, Fujian, China
[c] State Key Laboratory for Conservation and Utilization of Subtropical Agro-bioresources, South China Agricultural University, Guangzhou 510642, Guangdong, China

ARTICLE INFO

Article history:
Received 2 January 2025
Revised 7 March 2025
Accepted 8 March 2025
Available online 1 April 2025

Keywords:
Photorespiratory bypass
Photosynthetic Efficiency
Crop Yield
Rice

ABSTRACT

Photorespiration consumes photosynthetically fixed carbon and reduces yields by 20%–50% in C_3 crops. In an attempt to increase photosynthetic efficiency in rice by bypassing the carbon-consuming process of photorespiration, a photorespiratory bypass consisting of *Chlamydomonas reinhardtii* glycolate dehydrogenase and *Cucurbita maxima* malate synthase (termed the GMS bypass) was introduced into the rice cultivar Zhonghua 11 and *osplgg1b*, a mutant of the rice chloroplast glycolate transporter, to generate GMS/ZH11 and GMS/*osplgg1b* transgenic plants. The GMS bypass reduced photorespiration and increased photosynthesis in the transgenic plants. The straw biomass of GMS/ZH11 and GMS/*osplgg1b* increased by up to 16.0% and 85.7%, respectively. The yield of GMS/ZH11 increased by 22.0%–34.7% in paddy fields. Thus, the GMS bypass can increase photosynthetic efficiency and yield in rice.

1. Introduction

The light use efficiency in major crops under natural cultivation conditions is only 1% to 2%, which is lower than their theoretical maxima of 4.6% for C_3 plants and 6.0% for C_4 plants [1]. Photorespiration occurs concurrently with photosynthesis, serving primarily to eliminate 2-phosphoglycolate (2-PG), a byproduct of the Rubisco oxygenation reaction. 2-PG is a harmful compound that can inhibit the Calvin-Benson cycle and reduce photosynthetic efficiency [2,3]. In the photorespiratory cycle, the oxidation of glycine in mitochondria releases one molecule of CO_2, resulting in carbon loss. Photorespiration can consume 25%–30% of the photosynthetically fixed carbon in C_3 plants under normal growth conditions, increasing to up to 50% under environmental stresses such as elevated temperature, high light, and drought stress [4,5]. Given that the photorespiratory pathway involves a carbon-loss mechanism, optimization of photorespiration represents a promising avenue for increasing crop productivity [6,7].

Reconstruction of the photorespiratory pathway can elevate plant photosynthetic efficiency, biomass, and crop yields [8–13]. Among these photorespiratory bypasses, the synthetic glycolate metabolism pathways localized in the chloroplast are the most common [14,15]. The introduced glycolate oxidase (GOX) catalyzes the conversion of glycolate to glyoxylate, simultaneously producing hydrogen peroxide (H_2O_2) as a byproduct, necessitating the involvement of another enzyme, such as catalase or ascorbate peroxidase, to mitigate the toxic effects of H_2O_2 [9–13]. Alternatively, glycolate can be converted to glyoxylate through the action of a bacterial or algal glycolate dehydrogenase (GDH), a process that does not produce H_2O_2 [8,13]. In the subsequent stage, glyoxylate, in conjunction with acetyl-CoA, is converted to malate by a transgenic chloroplast-targeted malate synthase (MS). Malate is then successively converted to pyruvate and acetyl-CoA through the sequential activities of NADP-malic enzyme and pyruvate dehydrogenase, both of which are abundant in the chloroplasts of C_3 plants [9]. These reactions facilitate the release of CO_2 in the chloroplast, thereby establishing a CO_2 concentration mechanism that increases Rubisco carboxylation efficiency. For example, the *Chlamydomonas reinhardtii* GDH (CrGDH) and the *Cucurbita maxima* MS (CmMS) were integrated into tobacco chloroplasts to construct a photorespiratory bypass. RNA interference (RNAi) was used to reduce the expression of the chloroplast glycolate-glycerate transporter *PLGG1*, thereby minimizing the glycolate flux exiting the chloroplast and entering the native pathway [10]. The

* Corresponding author.
E-mail address: ghzhu@scau.edu.cn (G. Zhu).

https://doi.org/10.1016/j.cj.2025.03.001

synthetic pathways tested resulted in a 20% increase in photosynthetic quantum yield, and these transgenic tobacco plants exhibited over a 40% increase in biomass productivity during replicated field trials [10]. Inspired by this work, we wanted to investigate whether this photorespiratory bypass could similarly increase yield in rice.

The objective of this study was to identify the effects of CrGDH-CmMS photorespiratory bypass (referred to as GMS bypass) on rice growth and yield. The experimental strategy was to introduce the GMS bypass into a rice cultivar and an *osplgg1b* mutant in the same background. *osplgg1b* is a mutant of the rice glycolate transporter OsPLGG1b that shows a slight accumulation of glycolate in chloroplasts but no impairment of photosynthesis and growth [16,17]. We evaluated the effectiveness of the GMS bypass, as well as the photosynthetic efficiency, biomass, and yield of the GMS-transformed cultivars.

2. Materials and methods

2.1. Plant materials and growth conditions

Zhonghua 11 rice (*Oryza sativa* L., referred to as wild type, WT) was employed to generate GMS/ZH11 plants. Rice *osplgg1b*, a CRISPR/Cas9-edited variant derived from the ZH11 background [17], was used to generate GMS/*osplgg1b* plants. The germinated seeds were cultivated in Kimura B complete nutrient solution and grown in a greenhouse with a light intensity of 800–1000 μmol m^{-2} s^{-1}, a 14 h/10 h light/dark cycle, a temperature of 25–30 °C, and a relative humidity of 60%–80% for 21 d, after which they were transplanted into pots for further growth.

For field experiments, plants of the wild type and GMS rice were grown in Hainan paddy fields under natural conditions, with a planting density of 15 × 15 cm per plant. Each plot covered approximately 16 m^2 (4 m × 4 m). The plot yield was determined at harvest.

2.2. Construction of the GMS vectors and genetic transformation

The sequences of *CrGDH* and *CmMS* were obtained from NCBI (National Center for Biotechnology Information, USA), with certain codons within the *CrGDH* sequence being optimized, as illustrated in Fig. S1C. Following the artificial synthesis of these segments, an optimized chloroplast transit peptide RC2 [18] was appended to the 5′ terminus, and a GFP tag was incorporated at the 3′ end of both *CrGDH* and *CmMS*. Using Cre/loxP homologous recombination technology [19], the *RC2-CrGDH-GFP* fusion gene was inserted into the pYL322d1 vector, while the *RC2-CmMS-GFP* fusion gene was integrated into the pYL322d2 vector. These constructs were assembled into the multi-gene expression vector pBIA13. The expression of *RC2-CrGDH-GFP* was driven by the *NOS* promoter, whereas *RC2-CmMS-GFP* was driven by the *35S* promoter. The architecture of the GMS multi-gene expression vector is shown in Fig. 2B. The GMS multi-gene expression vector was introduced into rice ZH11 and *osplgg1b* mutants by *Agrobacterium*-mediated transformation using strain EHA105. Homozygous lines were selected based on hygromycin resistance, and PCR was used to confirm the presence of transgenes in individual plants. The primers used for vector construction are listed in Table S1.

2.3. Gene expression and protein detection

Total RNA was extracted from rice leaves and quality-checked and first-strand cDNA was synthesized with a cDNA synthesis kit. Quantitative real time (qRT)-PCR assay was performed using gene-specific primers with SYBR Premix ExTaq reagent (TaKaRa, Japan). *ACTIN* and *GAPDH* were used as internal controls. The primers used for qRT-PCR are listed in Table S1. Proteins were extracted from freshly harvested leaves and homogenized in an extraction buffer containing 0.5 mmol L^{-1} EDTA and 50 mmol L^{-1} PBS (pH 7.8). Equal amounts of protein (20 μg) were loaded and separated by SDS-PAGE, after which the proteins were transferred onto polyvinylidene fluoride membranes for Western blotting. The CrGDH and CmMS proteins were identified using an anti-GFP monoclonal antibody.

2.4. Assays of enzymatic activity

The *CrGDH* and *CmMS* genes were amplified and heterologously expressed in *E. coli* to produce recombinant proteins. The purified proteins were used to measure enzymatic activity. Proteins extracted from four-leaf stage GMS/ZH11 and GMS/*osplgg1b* leaves were used for GDH activity measurement. GDH and MS activity were assayed as described [20,21]. Primers used for prokaryotic expression are listed in Table S1.

2.5. Subcellular localization of CrGDH and CmMS

The coding sequences of *CrGDH* and *CmMS* were cloned into the pOX-RC2-GFP vector and transiently expressed in rice protoplasts. Protoplasts were extracted from the leaf sheaths of rice plants. The GFP signal was visualized under a confocal microscope (Leica sp5, Germany) 14 h after transformation. The primers used for vector construction are listed in Table S1.

2.6. Measurements of gas-exchange and chlorophyll fluorescence

An open flow gas exchange system (LI-6800, LI-COR, Lincoln, NE, USA) was used to measure the gas exchange parameters of the fully expanded flag leaf at the heading stage. The ambient CO_2 concentration in the LI-COR leaf chamber was controlled to 400 μmol mol^{-1}, the leaf temperature was maintained at 25 °C, the photosynthetic photon flux density (PFD) was set to 1200 μmol m^{-2} s^{-1}, and the flow rate was calibrated to 500 μmol s^{-1}.

The rate of photorespiration was determined by calculating the discrepancy in net photosynthetic rates (P_n) under conditions of low oxygen (2% O_2) and ambient oxygen (21% O_2). A compressed gas cylinder, containing a blend of 98% nitrogen and 2% oxygen, was connected to the LI-6800 air intake via a gas flow regulator. Following clamping, leaves were exposed to an incident PFD of 1200 μmol m^{-2} s^{-1} until full photosynthetic induction was achieved.

Light response curves were constructed under a leaf temperature of 25 °C, 60% relative humidity, and a CO_2 concentration of 400 μmol mol^{-1}, with the PFD systematically varied from 0 to 2000 μmol m^{-2} s^{-1} in increments of 100 μmol m^{-2} s^{-1}. These curves were then fitted using LI-COR software to determine the maximum net photosynthetic rate (A_{max}) and the light saturation point (LSP).

For CO_2 response curves, the CO_2 concentration was systematically adjusted to 20, 50, 100, 200, 300, 400, 600, 800, and 1000 μmol mol^{-1}, while a light intensity of 1200 μmol m^{-2} s^{-1} was maintained. The generation of A/C_i curves were conducted using the manufacturer's automated program. The apparent CO_2 compensation point was derived from the linear segment of the CO_2 response curves by regression.

Chlorophyll fluorescence parameters were measured with a portable chlorophyll fluorometer. Leaves were dark adapted for at least of 30 min prior to measurement of Y(Ⅱ), ETR, qP, and NPQ.

2.7. Phenotypic analysis and dry weight measurements

In seedlings at the three-leaf stage, shoot height, root length, and seedling weight were recorded. At maturity, plant height and tiller number were measured. Following harvest, panicle length, thousand-grain weight, straw weight, and grain weight were determined.

2.8. Transcriptome and metabolite measurements

Leaves from four-leaf stage ZH11 and GMS/ZH11 plants were used for RNA sequencing. RNA-seq reads were processed using StringTie [22]. Differentially expressed genes (DEGs) in ZH11 and GMS/ZH11 were identified with Metware (https://cloud.metware.cn). Gene differential expression between the two cultivars was conducted using DESeq2 [23]. A threshold of adjusted fold change (FC) ≥ 2 and P-value ≤ 0.05 was used to detect DEGs. Gene Ontology (GO) enrichment was performed using the R package [24]. RNA-Seq data for the heatmap were normalized by $\log_2$FC. The heatmap was generated using the TBtools software [25].

Targeted metabolomics assays were performed by UPLC-MS/MS using four-leaf stage ZH11 and GMS/ZH11 plants. Each sample was represented by three biological replicates. Metabolites were investigated by hierarchical cluster analysis (HCA), and heatmaps were generated using the ComplexHeatmap package in R software [26].

3. Results

3.1. Generation of the GMS photorespiratory bypass in ZH11 and osplgg1b plants

The CrGDH and CmMS were used to engineer a photorespiratory bypass. First, the *CrGDH* and *CmMS* gene sequences were stripped of their mitochondrial and peroxisomal signal peptides, respectively. The *CrGDH* codon was optimized to enhance expression in rice, and the sequences were then artificially synthesized. An optimized chloroplast transit peptide RC2 [18] was appended to the 5′ end of both genes (Fig. S1). The modified *CrGDH* and *CmMS* genes were then amplified and heterologously expressed in *E. coli*. Enzyme activity assays showed that these recombinant proteins possessed glycolate dehydrogenase and malate synthase activities, respectively (Fig. 1A), confirming their catalytic functions in vitro. Subsequently, plastids containing *CrGDH* or *CmMS* fused with green fluorescent protein (GFP) were constructed and transiently expressed in rice protoplasts. The detection of GFP fluorescence signals in the chloroplasts indicated that the RC2 signal peptide guided the proteins to the correct location (Fig. 1B).

To integrate the CrGDH-CmMS bypass (GMS bypass) into rice chloroplasts, the *CrGDH* gene, under the control of the *NOS* promoter, and the *CmMS* gene, driven by the *35S* promoter (Fig. 2A, B), were introduced into the ZH11 and *osplgg1b* mutant (ZH11 background). Following selection for hygromycin resistance, several independent homozygous transgenic lines were acquired, designated GMS/ZH11 and GMS/*osplgg1b*. Quantitative RT-PCR, RT-PCR and Western blot analyses of GMS/ZH11 and GMS/*osplgg1b* transgenic plants confirmed the overexpression of *CrGDH* and *CmMS* (Fig. 2C–E). GDH enzymatic activity was observed in all GMS plants (Fig. 2F), demonstrating the successful generation of the GMS photorespiratory bypass in rice.

3.2. Increased photosynthetic efficiency in GMS transgenic plants

The engineered GMS photorespiratory bypass induces partial glycolate degradation to CO_2 within the chloroplasts (Fig. 2A), thereby establishing a carbon-concentrating mechanism and improving the photosynthetic efficiency of rice. To determine whether the light reaction capacity was elevated, we assessed chlorophyll fluorescence in GMS transgenic plants at the four-leaf stage. The fully expanded second leaves were employed for rapid light curve measurements following a 30-min period of dark adaptation. In comparison to the wild type, most of the GMS transgenic lines exhibited an increase in the relative electron transport rate (ETR), the actual photochemical efficiency of photosystem II (Y (II)), and the photochemical quenching coefficient (qP) (Fig. S2).

To determine whether the CO_2 fixation capacity of the GMS transgenic lines has been bolstered, we conducted gas exchange measurements at the tillering stage. Diurnal variations in the photosynthetic rate of flag leaves was detected using a LI-6800 instrument (natural light intensity and CO_2 concentration of 400 μmol mol^{-1}). Relative to WT, the photosynthetic rates of GMS/ZH11 and GMS/*osplgg1b* plants increased, for instance, escalated by 13.5%–27.6% and 6.7%–22.2% at 14:00 PM, respectively (Fig. 3A). The intercellular CO_2 concentrations of the GMS/ZH11 and GMS/*osplgg1b* lines had risen by 3.6%–6.9% and 3.5%–10.0% (Fig. 3B),

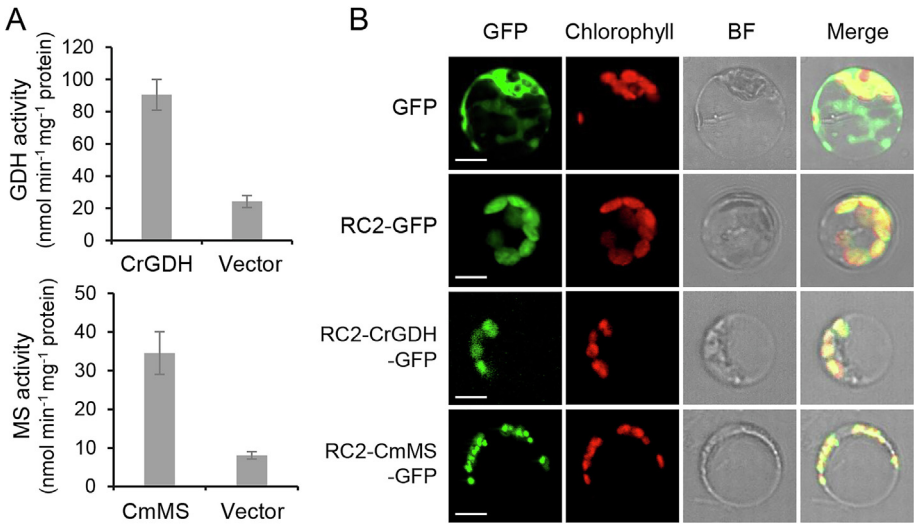

Fig. 1. Enzyme activity and subcellular localization of CrGDH and CmMS. (A) Enzyme activity assays of recombinant CrGDH and CmMS proteins. The crude extracts derived from empty vector transfected samples were used as controls. (B) Subcellular localization of CrGDH and CmMS. The *35S:CrGDH-GFP* and *35S:CmMS-GFP* constructs were transiently expressed in rice protoplasts for 14 h. GFP signals were observed by confocal microscopy. Scale bar, 5 μm.

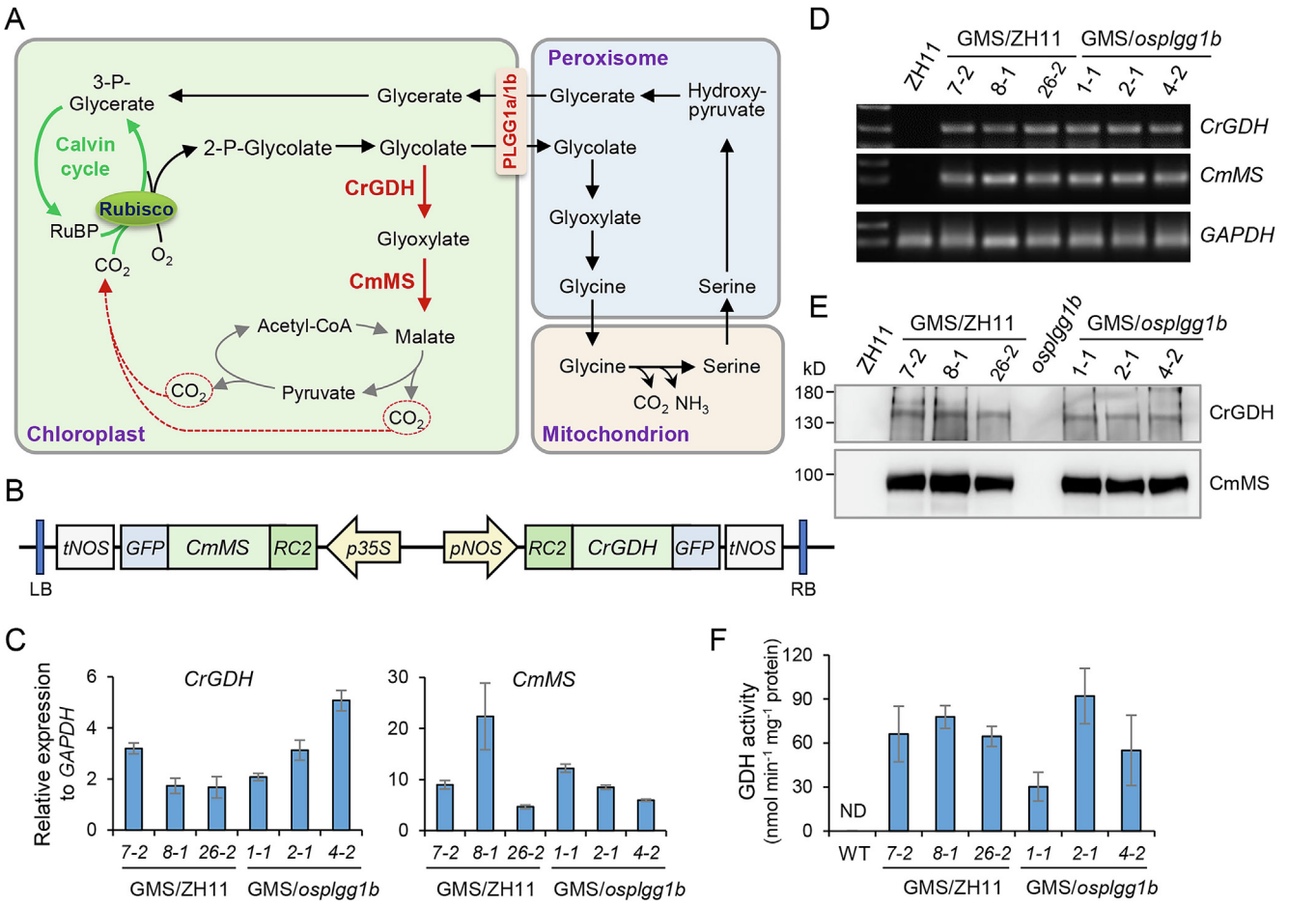

Fig. 2. Establishment of the GMS photorespiratory bypass in rice. (A) The designed GMS bypass (shown in red) is elucidated together with the natural photorespiratory pathway (shown in black). The introduced enzymes are highlighted in red. (B) Structure of the multi-gene expression vector. RC2 indicates a chloroplast transit peptide. (C–E) Transcrip and protein levels of CrGDH and CmMS in GMS transgenic plants. Total RNA and protein were extracted from the leaves of WT and GMS lines at the four-leaf stage for qRT-PCR (C), RT-PCR (D), and Western immunoblotting (E). GFP antibody was used for the Western blot analysis. (F) Assay of GDH enzymatic activityin GMS transgenic plants. Protein extracts from four-leaf stage leaves were used for enzyme activity quantification. Values are means ± SD (n = 5).

correspondingly, the photorespiration rates decreased by 8.8%–22.3% and 6.5%–15.4%, respectively (Fig. 3C), suggesting that the GMS photorespiratory bypass may have induced a mechanism for CO_2 concentration in the chloroplasts.

We also analyzed the light response and CO_2 response curves of the GMS transgenic lines during the tillering stage. The light response curves indicated that under relatively high light conditions (exceeding 1000 μmol m^{-2} s^{-1}), the net photosynthetic rates (P_n) of the GMS transgenic lines exceeded those of the WT, particularly for the GMS/*osplgg1b* lines (Fig. 3D). The maximum photosynthetic rates of GMS/ZH11 and GMS/*osplgg1b* lines increased by 5.1%–10.4% and 8.7%–18.1%, respectively (Fig. 3E), and the light saturation points increased by 2.2%–13.2% and 10.7%–25.4%, respectively, in contrast to WT (Fig. 3F). The CO_2 response curve illustrated that the P_n of the GMS transgenic lines exceeded that of the WT when CO_2 concentrations are greater than 400 μmol mol^{-1} (Fig. 3G). Surprisingly, the CO_2 compensation points of the GMS/ZH11 and GMS/*osplgg1b* lines also increased by 9.8%–18.5% and 4.2%–15.0%, respectively (Fig. 3H), which may be attributed to the increased decarboxylation resulting from the introduced GMS photorespiratory bypass. Collectively, these results demonstrate that the GMS photorespiratory bypass increases the light use efficiency and CO_2 fixation capacity of transgenic rice.

3.3. Growth performance of GMS transgenic plants

To determine whether the enhanced photosynthetic capacity could increase rice growth, we quantified relevant parameters of the GMS transgenic lines at both the seedling and mature stages. Plants were cultivated in pots under environmental light conditions (light intensity approximately 1000–1600 μmol m^{-2} s^{-1} during daylight hours). In comparison with the wild type, the GMS transgenic rice exhibited significant growth advantages (Fig. 4A, B). For example, the plant height of the GMS/ZH11 and GMS/*osplgg1b* lines increased by 27.3%–33.5% and 11.6%–20.7% (Fig. 4C), and the fresh weight per plant increased by 23.0%–30.0% and 1.1%–8.3%, respectively, at the seedling stage (Fig. 4D). The SPAD values for the GMS/ZH11 and GMS/*osplgg1b* lines increased by 1.3%–7.6% and 6.1%–14.0%, respectively, at the heading stage (Fig. 4E). The number of effective tillers also increased in GMS transgenic plants, particularly in the GMS/*osplgg1b* lines (Fig. 4B). Consequently, the dry weight of straw of GMS/ZH11 lines increased by 35.4%–49.9%, and that of GMS/*osplgg1b* lines by 15.8%–62.6% (Fig. 4F), indicating that the GMS photorespiratory bypass enhances biomass productivity. Nonetheless, we observed a reduction in seed setting rates in the GMS/*osplgg1b* lines, a trend that was also observed when cultivated in paddy fields.

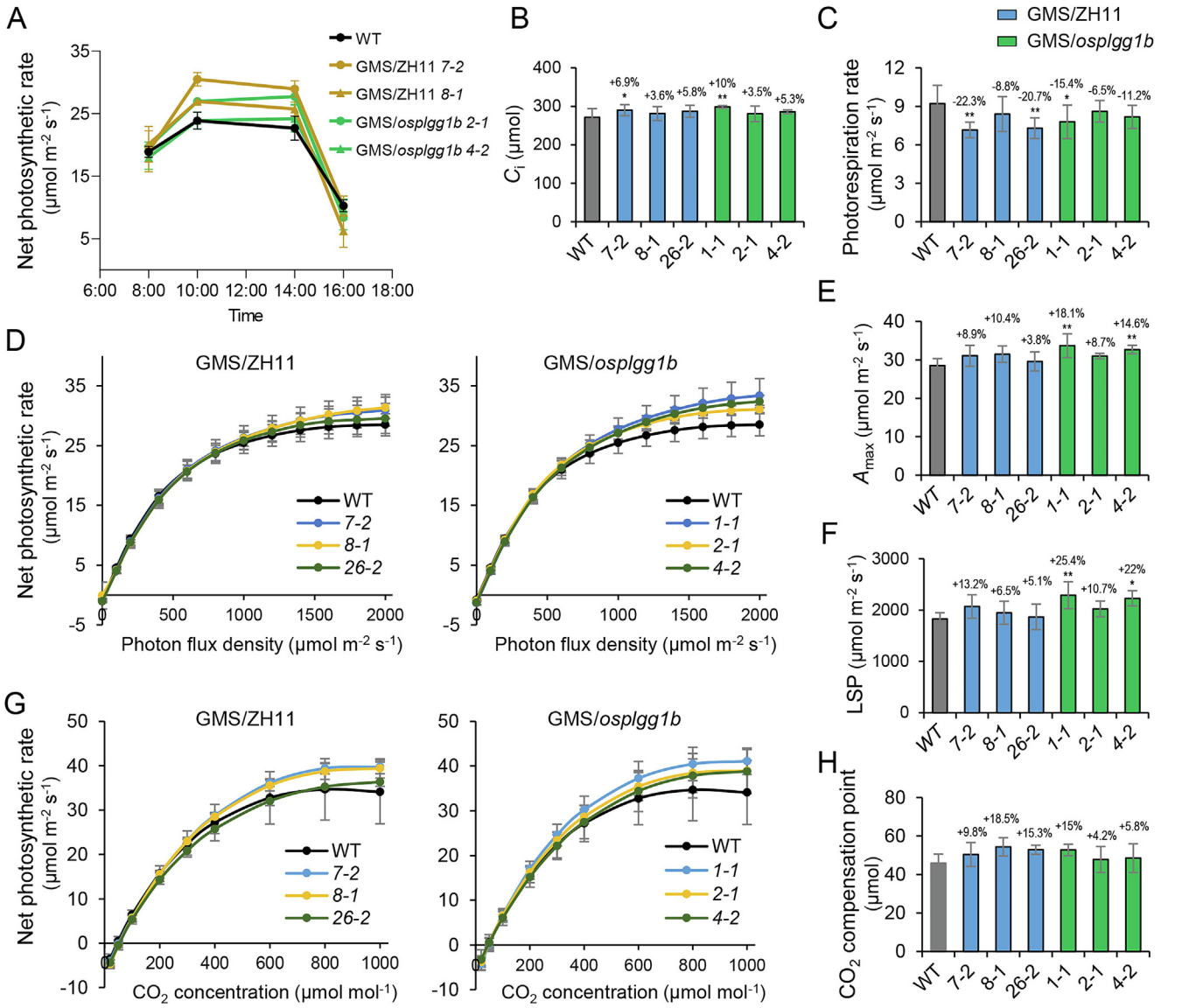

Fig. 3. Gas-exchange measurements in GMS transgenic plants. (A) Diurnal curves of the net photosynthetic rate in GMS transgenic plants. (B, C) Intercellular CO_2 concentration (C_i) and the photorespiration rate of GMS transgenic plants (n > 10). (D) Light response curves were generated at a temperature of 28 °C and a CO_2 concentration of approximately 400 μmol mol^{-1} (n = 8). (E, F) The light-saturated photosynthetic rate (A_{max}) and the light saturation point (LSP) were calculated from the light response curves. (G) The CO_2 response curves were generated at a PFD of 1200 μmol m^{-2} s^{-1} and a temperature of 28 °C (n = 6). (H) CO_2 compensation point was measured using the Laisk method. Plants were grown in pots with paddy soil under greenhouse conditions. All measurements were performed using the flag leaf of rice at the heading stage. Values are means ± SD. Asterisks indicate a significant difference compared with ZH11 (*, P < 0.05; **, P < 0.01 by Student's t-test).

3.4. Yield performance of GMS transgenic rice in paddy fields

We carried out paddy field trials to assess the agronomic and yield traits of GMS transgenic rice (Fig. 5A). The GMS/ZH11 lines exhibited an increment of plant height of 6.4%–10.1% relative to the WT, while the GMS/*osplgg1b* lines showed no significant change (Fig. 5B). Consistent with observations in potted plants, the GMS transgenic lines showed increased tillers, particularly the GMS/*osplgg1b* lines, with an increase of 24.5%–86.0% over the WT (Fig. 5C). Compared to the WT, the main panicle length of the GMS/ZH11 lines significantly elongated by 4.4%–13.0%, along with an increase in the number of grains per panicle (Fig. 5A, D). Grain length and thousand-grain weight also increased, especially for the GMS/ZH11-*7-2* line (Figs. 5E, S3). Ultimately, the straw biomass and grain yield per plant increased by 1.8%–16.0% and 22.0%–34.7%, respectively, in the GMS/ZH11 lines (Fig. 5G, H). No significant discrepancies were observed in the main panicle length and thousand-grain weight of the GMS/*osplgg1b* lines compared to the WT, however, their setting rates experienced a pronounced reduction of 14.4%–33.1% (Fig. 5D, F). Thus, while the individual plant straw biomass of the GMS/*osplgg1b* lines increased by 15.4%–85.7%, there was no significant difference in grain yield (Fig. 5G, H). Straw biomass and grain yield in field plots were consistent with individual plant assessments (Fig. S4).

3.5. Transcriptome and metabolite analysis of GMS/ZH11 transgenic plants

Given the notable enhancement in photosynthetic efficiency, biomass, and yield observed in GMS/ZH11 plants, we delved deeper into elucidating the underlying mechanisms. Leaves from four-leaf stage wild-type and GMS/ZH11-*7-2* plants were subjected to comprehensive transcriptome and metabolomics analyses. The study incorporated three independent biological replicates.

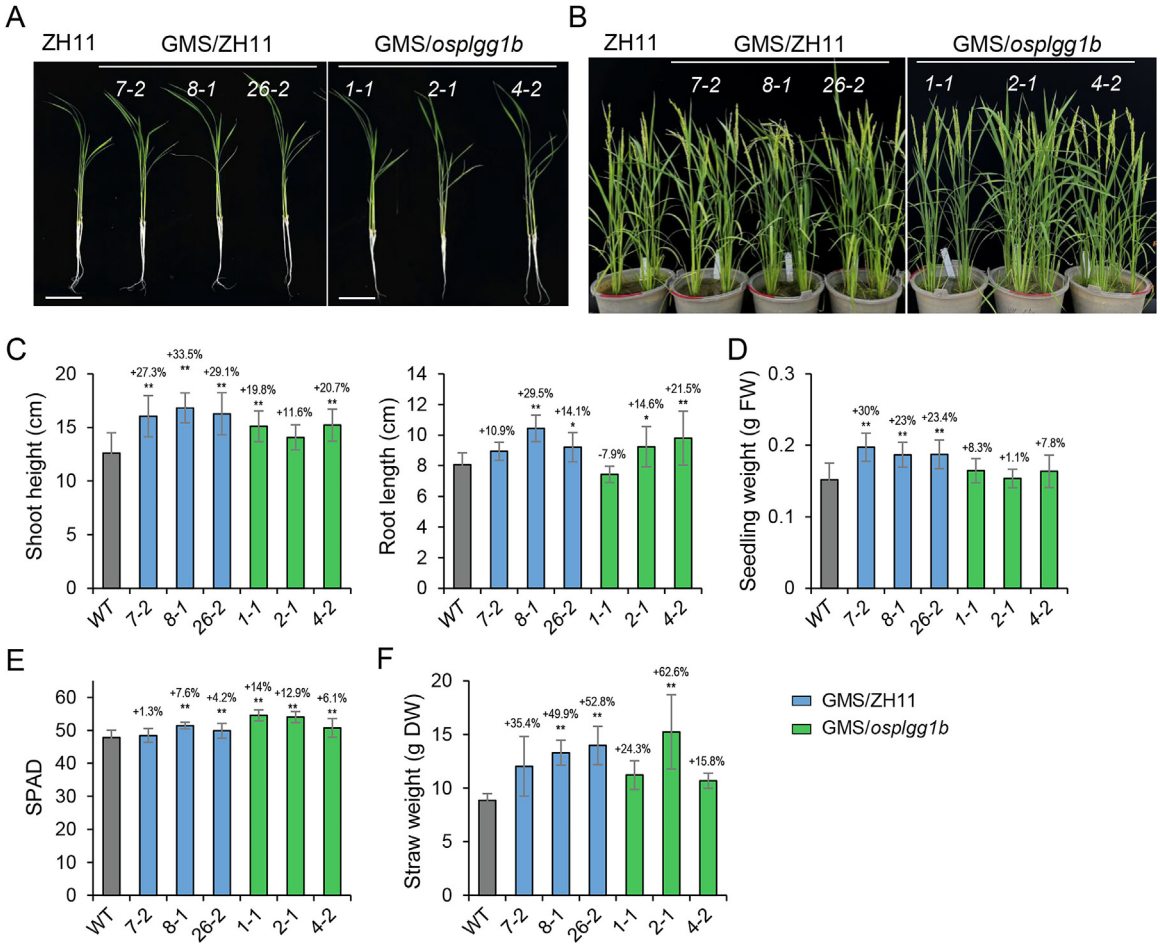

Fig. 4. Growth performance of GMS transgenic plants. (A, B) Representative images depicting GMS transgenic plants at the seedling stage (A) and the heading stage (B). (C) Measurements of shoot height and root length of GMS transgenic plants grown at the seedling stage. (D) Fresh biomass weight of GMS transgenic plants at the seedling stage. (E) SPAD values of GMS transgenic plants at the heading stage. (F) Straw mass of GMS transgenic plants at the mature stage. These parameters were obtained from pot-grown plants. Values are means ± SD (n > 10). Asterisks indicate a significant difference compared to ZH11 (*, P < 0.05; **, P < 0.01 by Student's t-test).

RNA sequencing revealed the identification of 908 differentially expressed genes (DEGs, fold change ≥ 2, P-value ≤ 0.05), with 431 genes being up-regulated and 477 genes being down-regulated in the GMS/ZH11-7-*2* plants relative to the wild type (Fig. 6A; Dataset S1-1, S1-2). Gene Ontology (GO) analysis of these DEGs highlighted that the most enriched genes were associated with the biological processes of growth regulation (GO:0046620), photosynthesis (GO:0015979), hormone metabolic process (GO:0042445), nitrate assimilation (GO:0042128), and photorespiration (GO:0009853) (Fig. 6B). In consonance with this, analysis of cellular components (GO-C) indicated that these DEGs were predominantly localized to the chloroplast thylakoid membrane (GO:0009535) and the plastid thylakoid membrane (GO:0055035) (Fig. 6B). A group of genes essential for photosynthesis and starch biosynthesis were observed to be up-regulated in the GMS/ZH11-7-*2* plants, including the genes *OsRBCS* genes for CO_2 assimilation, *OsFBP1* and *OsSBPase* for the Calvin-Benson cycle, *Wx*, *OsSSIIb*, and *OsSSIIIb* for starch biosynthesis, and *OsNR1.1*, *OsGS2*, and *OsFd-GOGAT* for nitrate assimilation (Fig. 6C; Dataset S1-3). These observations suggest an increased capacity for carbon assimilation in the GMS/ZH11 plants.

Targeted metabolomics was conducted using the UPLC-MS/MS system. A total of 66 metabolites, including nucleotides and their metabolites, amino acids, organic acids and their derivatives, and carbohydrates and phosphate sugars, were quantitatively analyzed (Table S2). Among these metabolites, several intermediates crucial for the Calvin-Benson cycle and starch biosynthesis were found to be significantly accumulated in the GMS/ZH11-7-*2* plants, in particular ribulose 1,5-bisphosphate (RuBP), 3-phosphoglycerate (3-PGA), fructose-6-phosphate (F6P), glucose-6-phosphate (G6P), and glucose-1-phosphate (G1P) (Fig. 7A, B), findings that corroborated the results of the transcriptome analysis (Fig. 7B). We also assessed the soluble sugar and starch content in the GMS transgenic plants at the heading stage. GMS/ZH11 plants did not differ in soluble sugar content compared to the wild type, while an increase of 25.6%–63.1% in starch content was observed (Fig. 7C). In addition, both soluble sugar and starch contents were notably elevated in the GMS/*osplgg1b* lines (Fig. 7C).

4. Discussion

4.1. Successful engineering of a GMS photorespiratory bypass in rice

Recent efforts using synthetic biology to reconstruct photorespiratory bypasses have demonstrated substantial advances in photosynthetic efficiency, biomass, and crop yields [14,15]. The conversion of glycolate to glyoxylate in chloroplasts is a pivotal step in the construction of most synthetic photorespiratory bypasses. In higher plants, this reaction is catalyzed by glycolate oxidase (GLO), which employs molecular oxygen as a co-substrate, leading to the generation of hydrogen peroxide (H_2O_2). Consequently, these bypass systems necessitate the expression of

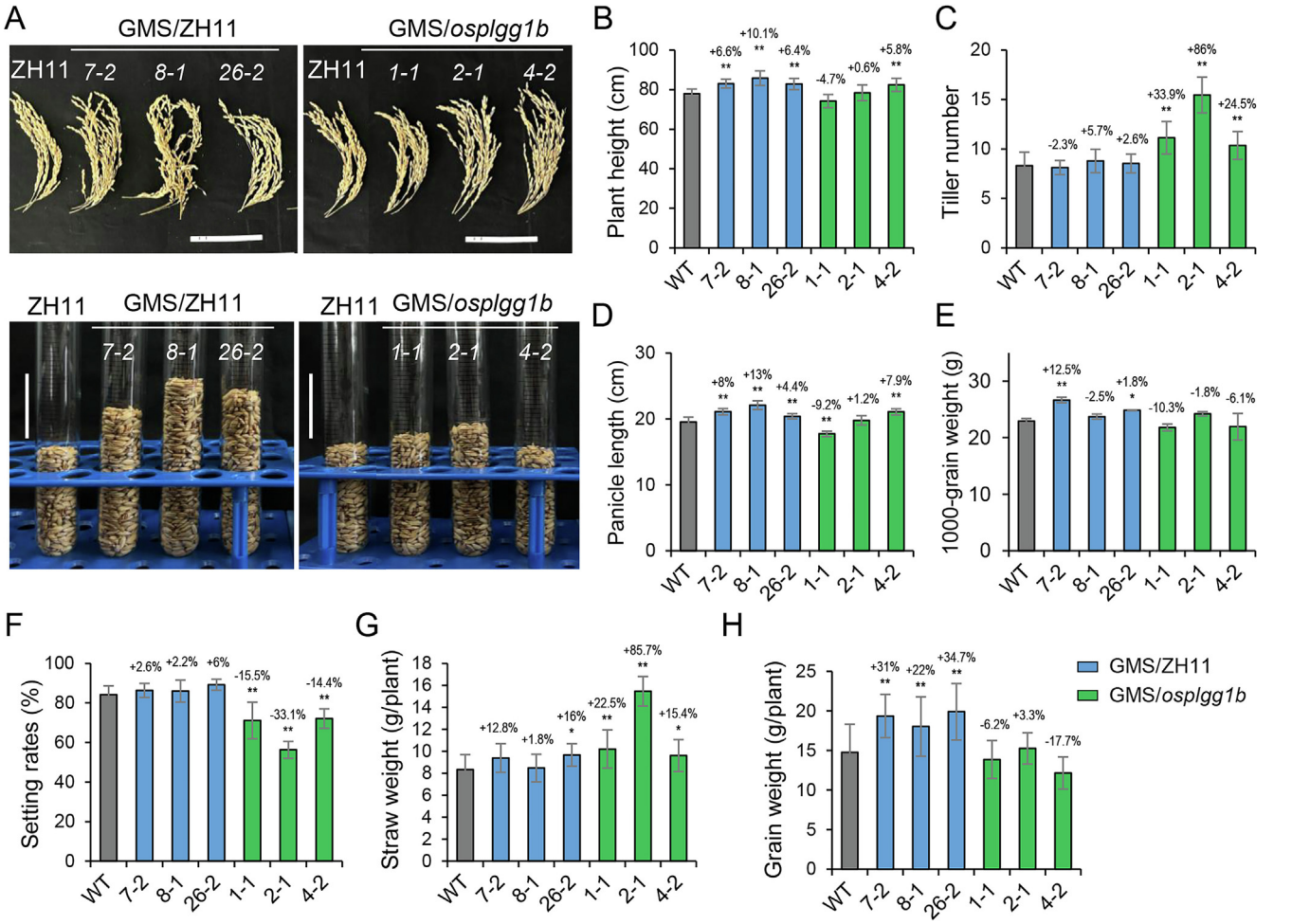

Fig. 5. Biomass and yield performance of GMS transgenic rice in paddy fields. (A) Representative photographs of main panicle morphology of GMS transgenic rice. (B–H) Quantification of plant height (B), tiller number (C), panicle length (D), 1000-grain weight (E), setting rate (F), straw weight per plant (G), and grain weight per plant (H). Plants were grown in the field. Values are means ± SD (n = 5 for (E), and n > 30 for others). Asterisks indicate a significant difference compared to ZH11 (*, $P < 0.05$; **, $P < 0.01$ by Student's t-test).

enzymes capable of metabolizing H_2O_2, such as catalase (CAT) and ascorbate peroxidase (APX) [9,11–13]. In contrast, in bacteria and algae, the same step is facilitated by glycolate dehydrogenase (GDH), which operates with NAD^+ as its coenzyme, thereby eliminating the production of H_2O_2 and circumventing its deleterious effects on plant growth [8,10]. For instance, tobacco plants engineered to express *CrGDH* and *CmMS*, coupled with a reduction in *PLGG1* expression through RNA interference, showed a marked increase in biomass productivity in replicated field trials [10].

In this study, a GDH-MS photorespiratory bypass was engineered in the rice cultivar ZH11 and the *osplgg1b* mutant, as evidenced by the following: First, assessments at the level of mRNA, protein expression, and enzymatic activity confirmed the presence and functionality of CrGDH and CmMS in the transgenic lines (Fig. 2). Second, an increase in the intracellular CO_2 concentration was observed in the transgenic lines compared to the wild type, accompanied by a reduction in the photorespiration rate, with some lines showing a decrease of more than 20% (Fig. 3). The increase of the CO_2 compensation point in the transgenic lines, a finding not previously reported for engineered bypasses [11,12], can be explained by the increased CO_2 release associated with the GDH-MS photorespiratory bypass. Theoretically, the decarboxylation of a single glycolate molecule rerouted within the chloroplast yields two molecules of CO_2, whereas the decarboxylation of glycolate in the native photorespiratory pathway results in the production of only half a molecule of CO_2 [27]. Third, comprehensive transcriptomic and metabolomic analyses revealed an induction of a suite of genes relevant to photosynthesis and starch biosynthesis in the GMS/ZH11 plants, a pattern mirrored by the notable accumulation of several intermediates of the Calvin-Benson cycle and starch (Figs. 6, 7). Collectively, these findings provide compelling evidence for the successful engineering of a GMS photorespiratory bypass in rice.

4.2. GMS bypass increases photosynthetic efficiency and productivity in rice

Our results indicate that the GMS photorespiratory bypass can enhance the photosynthetic efficiency of rice. Analysis of the light-response and CO_2-response curves revealed an increased photosynthetic rate in GMS lines, particularly under conditions of elevated light intensity and CO_2 concentration (Fig. 3D–G), which is likely attributable to elevated CO_2 levels in chloroplasts, thereby establishing a CO_2-concentrating mechanism and increasing the carboxylation efficiency of Rubisco [27]. An increase in chlorophyll content was observed in the GMS lines, particularly in the GMS/*osplgg1b* lines (Fig. 4E), potentially expanding the light-harvesting antenna system and amplifying light energy absorption [28,29]. For instance, we observed improvements in Y(II), ETR, and qP in comparison to wild-type plants (Fig. S2); thus, the increased

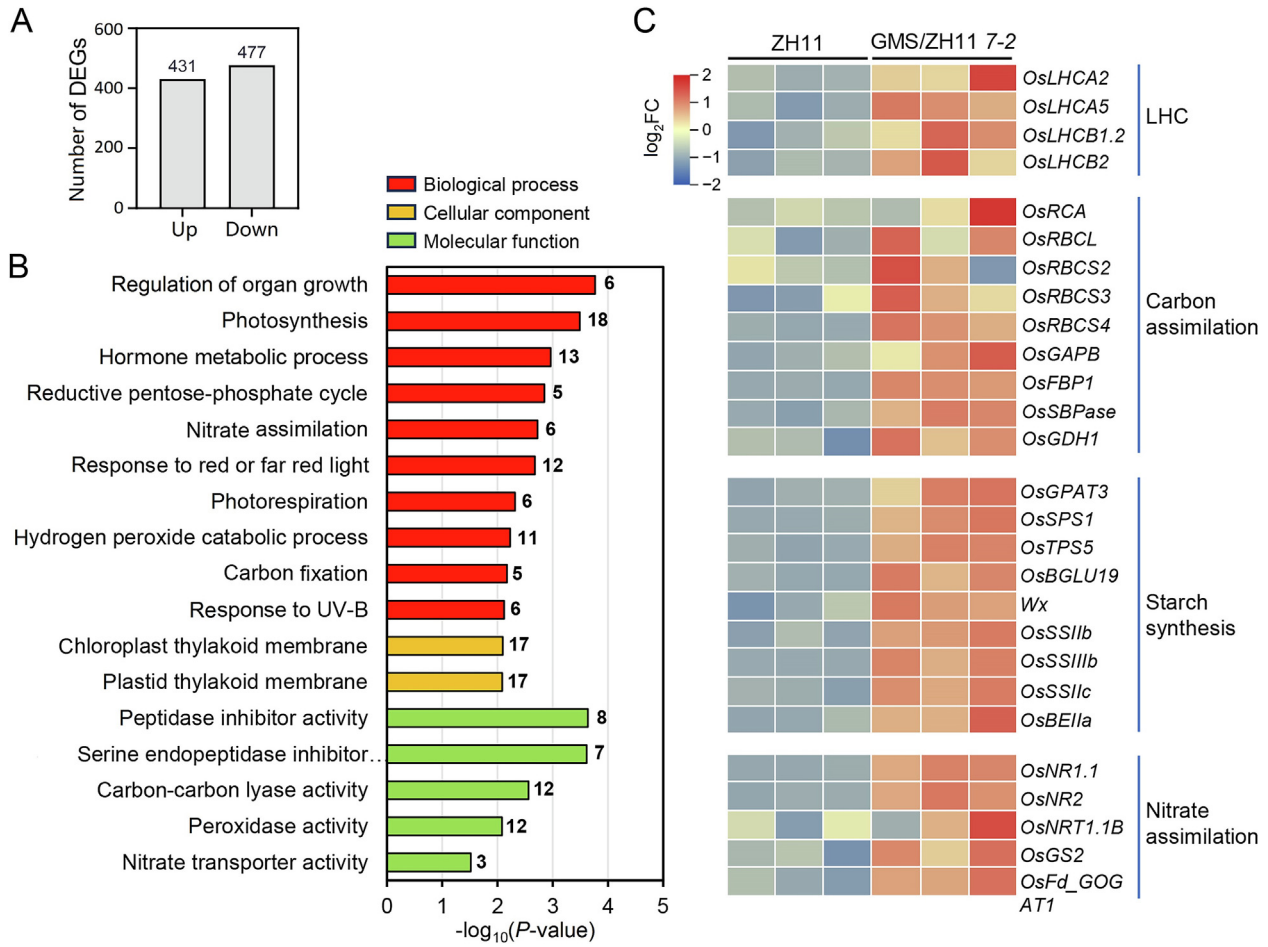

Fig. 6. Transcriptome analysis of GMS/ZH11 transgenic rice. (A) Differentially expressed genes (DEGs) between ZH11 and GMS/ZH11. RNA sequencing was performed using four-leaf stage leaves. Results are from three biological replicates. (B) Gene ontology (GO) analysis of DEGs between ZH11 and GMS/ZH11. The *Y*-axis denotes the corresponding GO term, the *X*-axis denotes the $-\log_{10}$ corresponding to the *P*-value of that GO term, and the numbers in the graph denote the number of genes enriched for the corresponding GO term. (C) Comparison of expression levels of genes related to LHC, carbon assimilation, starch synthesis and nitrate assimilation in ZH11 and GMS/ZH11 plants. Values are expressed as $\log_2$FC.

absorption and conversion of light energy, coupled with a more efficient CO_2 assimilation process, bolstered the photosynthetic efficiency of the GMS transgenic plants.

The introduced GMS bypass increased photosynthetic carbon assimilation. For instance, several *OsRBCS* genes encoding the small subunit of Rubisco were upregulated in GMS/ZH11 plants (Fig. 6C), potentially increasing Rubisco content and carboxylation activity [30]. Consistent with this, metabolic profiling revealed a pronounced accumulation of 3-phosphoglycerate (Fig. 7A), indicative of an elevated carbon assimilation capacity. Several key genes involved in starch biosynthesis, such as *OsAPL4* and *OsSSIIs*, were upregulated in GMS/ZH11 plants, corresponding to increased levels of phosphorylated intermediates in the starch biosynthesis pathway, including fructose-6-phosphate, glucose-6-phosphate, and glucose-1-phosphate (Fig. 7B), thus suggesting the activation of starch biosynthesis pathway [31–33]. We noted an upregulation in a cluster of genes associated with nitrogen assimilation, including *OsNR1.1*, *OsGS2*, and *OsFd-GOGAT*, in the GMS/ZH11 plants (Fig. 6C). We posit that the altered carbon assimilation dynamics in the GMS pathway may coordinate the regulation of nitrogen metabolism, mirroring the carbon–nitrogen coupling effects evident in the GCBG photorespiratory bypass pathway [34]. Collectively, these observations suggest that the GMS pathway promotes a synergistic enhancement of photosynthetic carbon assimilation, nitrogen utilization, and starch biosynthesis.

Optimizing the use of light energy and enhancing carbon assimilation could lead to improvements in photosynthetic efficiency, potentially resulting in increased agricultural productivity [35–37]. Consistently, our results suggest that the GMS photorespiratory bypass facilitates rice growth and increases productivity (Figs. 4, 5). For example, the GMS/ZH11 line exhibited more robust growth at the seedling stage and attained greater plant height at maturity; in particular, the tiller number of GMS/*osplgg1b* plants increased significantly (Figs. 4B, 5C). Consequently, the aboveground biomass, comprising straw and grain, of the GMS lines exhibited a substantial increase in both pot and field trials (Figs. 4F, 5G, H). These observations are consistent with previous reports on GDH-MS photorespiratory bypasses, such as the CrGDH-CmMS bypass in tobacco and the CrGDH-ChMS bypass in poplar, which synergistically improve plant photosynthetic efficiency and biomass [10,38].

Notably, while field experiments revealed a 22.0%–34.7% yield enhancement in GMS/ZH11 plants, no substantial increase was observed in the GMS/*osplgg1b* plants, possibly due to a marked reduction in seed setting rate (Fig. 5F–H). Analogous phenomena have been documented with GOC and GCGT photorespiratory bypasses, where superior photosynthetic efficiency correlates with reduced seed set [11,12]. A plausible explanation is that the deficiency of *OsPLGG1b* expression in GMS/*osplgg1b* plants results in a greater accumulation of glycolate within chloroplasts, thereby

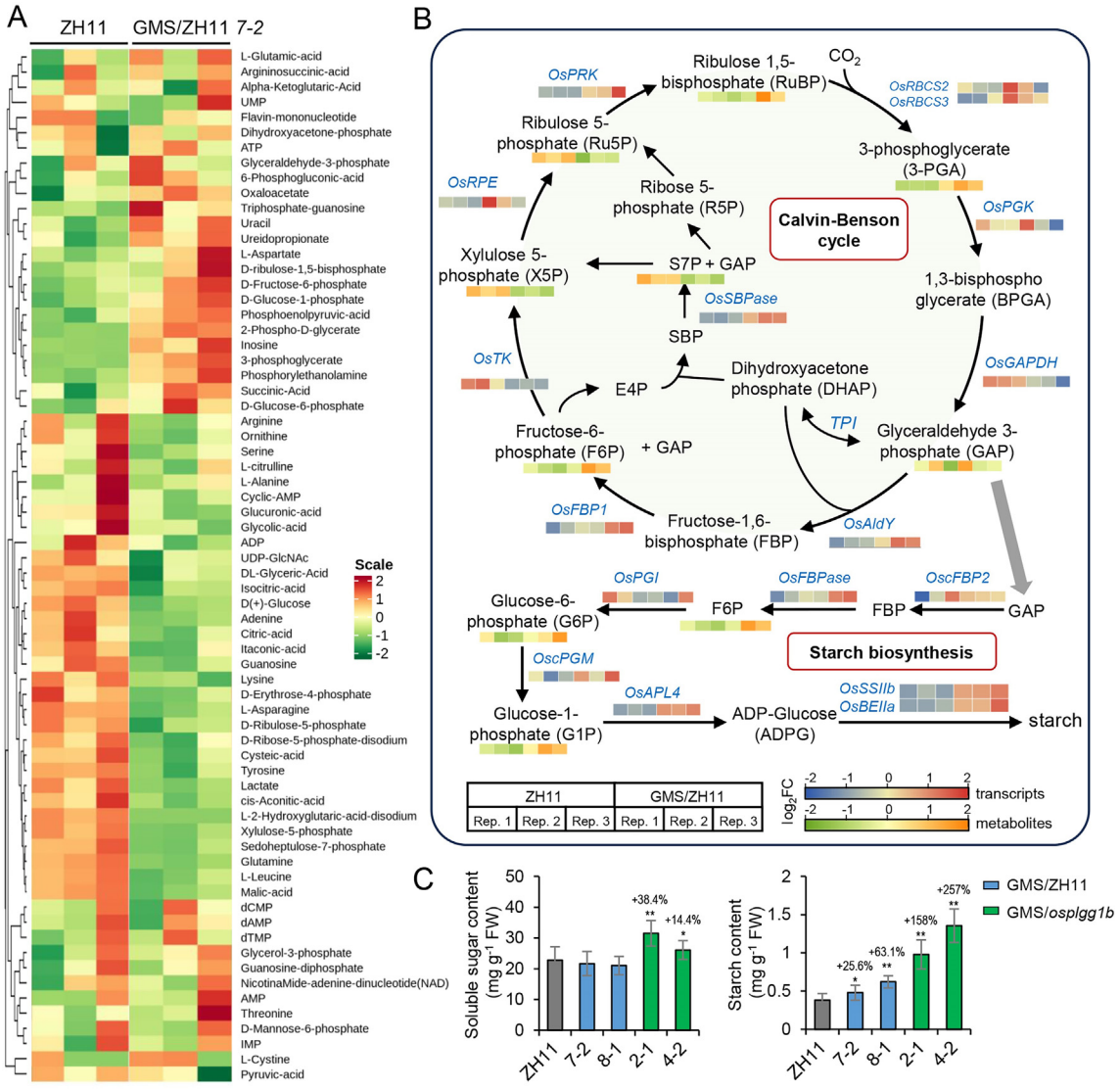

Fig. 7. Metabolomic analysis of GMS/ZH11 transgenic rice. (A) Hierarchical cluster analysis (HCA) of metabolites by heatmaps. Normalized signal intensities of metabolites are visualized as a color spectrum. Red indicates high abundance and green indicates low abundance. Metabolites were quantified in leaves at the four-leaf stage. The data presented are derived from three biological replicates. (B) Transcript levels and metabolite contents associated with the Calvin-Benson cycle and starch biosynthesis pathways in ZH11 and GMS/ZH11 plants. *OsRBCS2* (Os12g0274700), *OsRBCS3* (Os12g0291400), *OsPGK* (Os06g0668200), *OsFBP1* (Os01g0866400), *OsRPE* (Os03g0169100), *OsFBPase* (Os03g0267300), *OsAldY* (Os06g0608700), *OsGAPDH* (Os08g0126300), *OscPGM* (Os03g0712700), *OsSSIIb* (Os02g0744700), *OsBEIIa* (Os04g0409200), *OsSBPase* (Os04g0234600), *OsPRK* (Os02g0698000), *OsPGI* (Os08g0478800), *OsTK* (Os04g0266900), *OsAPL4* (Os07g0243200), *OscFBP2* (Os05g0438600). (C) Contents of soluble sugars and starch in GMS transgenic plants at the heading stage. Values are means ± SD ($n > 8$). Asterisks indicate a significant difference compared with ZH11 (*, $P < 0.05$; **, $P < 0.01$ by Student's *t*-test,).

amplifying the benefits of the GDH-MS bypass, for instance, greater photosynthetic capacity and increased starch accumulation were observed in the leaves of GMS/*osplgg1b* plants compared to those of GMS/ZH11 (Figs. 3, 7C). In addition, the constitutive expression of GDH-MS may disturb the "source-sink-flow" balance of the plant, especially during the night period. A comparable case is the expression of the photorespiratory gene *GDC-H* under the control of a light-inducible promoter (ST-LS1) in tobacco, which promotes growth rate and biomass, whereas the use of a constitutive promoter has negative effects [39]. Therefore, a light-inducible GDH-MS bypass should be explored to achieve better growth and yield performance in the future.

CRediT authorship contribution statement

Xiangze Chen: Investigation. **Guangru Li:** Data curation. **Haohui He:** Investigation. **Wenle Xie:** Investigation. **Lili Cui:** Investigation. **Zhisheng Zhang:** Data curation. **Xinxiang Peng:** Supervision, Conceptualization. **Guohui Zhu:** Writing – original draft, Conceptualization.

Declaration of competing interest

The authors declare that they have no known competing financial interests or personal relationships that could have appeared to influence the work reported in this paper.

Acknowledgments

This work was supported by the National Key Research and Development Program of China (2020YFA0907600), the Biological Breeding-National Science and Technology Major Project (2024ZD04080), the National Natural Science Foundation of China

(32270252), and the Natural Science Foundation of Guangdong Province (2024A1515011085).

Appendix A. Supplementary data

Supplementary data for this article can be found online at https://doi.org/10.1016/j.cj.2025.03.001.

References

[1] X.G. Zhu, S.P. Long, D.R. Ort, Improving photosynthetic efficiency for greater yield, Annu. Rev. Plant Biol. 61 (2010) 235–261.

[2] F. Flügel, S. Timm, S. Arrivault, A. Florian, M. Stitt, A.R. Fernie, H. Bauwe, The photorespiratory metabolite 2-phosphoglycolate regulates photosynthesis and starch accumulation in Arabidopsis, Plant Cell 29 (2017) 2537–2551.

[3] J. Li, S.M. Weraduwage, A.L. Preiser, S. Tietz, S.E. Weise, D.D. Strand, J.E. Froehlich, D.M. Kramer, J. Hu, T.D. Sharkey, A cytosolic bypass and G6P shunt in plants lacking peroxisomal hydroxypyruvate reductase, Plant Physiol. 180 (2019) 783–792.

[4] F.A. Busch, Current methods for estimating the rate of photorespiration in leaves, Plant Biol. 15 (2013) 648–655.

[5] B.J. Walker, A. Vanloocke, C.J. Bernacchi, D.R. Ort, The costs of photorespiration to food production now and in the future, Annu. Rev. Plant Biol. 67 (2016) 107–129.

[6] M. Hagemann, H. Bauwe, Photorespiration and the potential to improve photosynthesis, Curr. Opin. Chem. Biol. 35 (2016) 109–116.

[7] P.F. South, A.P. Cavanagh, P.E. López-Calcagno, C.A. Raines, D.R. Ort, Optimizing photorespiration for improved crop productivity, J. Integr. Plant Biol. 60 (2018) 1217–1230.

[8] R. Kebeish, M. Niessen, K. Thiruveedhi, R. Bari, H.J. Hirsch, R. Rosenkranz, N. Stäbler, B. Schönfeld, F. Kreuzaler, C. Peterhansel, Chloroplastic photorespiratory bypass increases photosynthesis and biomass production in *Arabidopsis thaliana*, Nat. Biotechnol. 25 (2007) 593–599.

[9] A. Maier, H. Fahnenstich, S. von Caemmerer, M.K.M. Engqvist, A.P.M. Weber, U. Flügge, V.G. Maurino, Transgenic introduction of a glycolate oxidative cycle into *A. Thaliana* chloroplasts leads to growth improvement, Front. Plant Sci. 3 (2012) 38.

[10] P.F. South, A.P. Cavanagh, H.W. Liu, D.R. Ort, Synthetic glycolate metabolism pathways stimulate crop growth and productivity in the field, Science 363 (2019) eaat9077.

[11] B. Shen, L. Wang, X. Lin, Z. Yao, H. Xu, C. Zhu, H. Teng, L. Cui, E.E. Liu, J. Zhang, Z. He, X. Peng, Engineering a new chloroplastic photorespiratory bypass to increase photosynthetic efficiency and productivity in rice, Mol. Plant 12 (2019) 199–214.

[12] L. Wang, B. Shen, B. Li, C. Zhang, M. Lin, P. Tong, L. Cui, Z. Zhang, X. Peng, A synthetic photorespiratory shortcut enhances photosynthesis to boost biomass and grain yield in rice, Mol. Plant 13 (2020) 1802–1815.

[13] H. Xu, H. Wang, Y. Zhang, X. Yang, S. Lv, D. Hou, C. Mo, M. Wassie, B. Yu, T. Hu, A synthetic light-inducible photorespiratory bypass enhances photosynthesis to improve rice growth and grain yield, Plant Commun. 4 (2023) 100641.

[14] A.R. Fernie, H. Bauwe, Wasteful, essential, evolutionary stepping stone? The multiple personalities of the photorespiratory pathway, Plant J. 102 (2020) 666–677.

[15] K. Jin, G. Chen, Y. Yang, Z. Zhang, T. Lu, Strategies for manipulating Rubisco and creating photorespiratory bypass to boost C_3 photosynthesis: prospects on modern crop improvement, Plant Cell Environ. 46 (2023) 363–378.

[16] S.H. Shim, S.K. Lee, D.W. Lee, D. Brilhaus, G. Wu, S. Ko, C.H. Lee, A.P.M. Weber, J. S. Jeon, Loss of function of rice plastidic glycolate/glycerate translocator 1 impairs photorespiration and plant growth, Front. Plant Sci. 10 (2019) 1726.

[17] L. Cui, C. Zhang, Z. Li, T. Xian, L. Wang, Z. Zhang, G. Zhu, X. Peng, Two plastidic glycolate/glycerate translocator 1 isoforms function together to transport photorespiratory glycolate and glycerate in rice chloroplasts, J. Exp. Bot. 72 (2021) 2584–2599.

[18] B.R. Shen, C.H. Zhu, Z. Yao, L.L. Cui, J.J. Zhang, C.W. Yang, Z.H. He, X.X. Peng, An optimized transit peptide for effective targeting of diverse foreign proteins into chloroplasts in rice, Sci. Rep. 7 (2017) 46231.

[19] Q. Zhu, S. Yu, D. Zeng, H. Liu, H. Wang, Z. Yang, X. Xie, R. Shen, J. Tan, H. Li, X. Zhao, Q. Zhang, Y. Chen, J. Guo, L. Chen, Y.G. Liu, Development of "purple endosperm rice" by engineering anthocyanin biosynthesis in the endosperm with a high-efficiency transgene stacking system, Mol. Plant 10 (2017) 918–929.

[20] J.M. Lord, Glycolate oxidoreductase in *Escherichia coli*, Biochim. Biophys. Acta-Bioenerg. 267 (1972) 227–237.

[21] H. Fahnenstich, T.E. Scarpeci, E.M. Valle, U. Flügge, V.G. Maurino, Generation of hydrogen peroxide in chloroplasts of Arabidopsis overexpressing glycolate oxidase as an inducible system to study oxidative stress, Plant Physiol. 148 (2008) 719–729.

[22] M. Pertea, G.M. Pertea, C.M. Antonescu, T. Chang, J.T. Mendell, S.L. Salzberg, StringTie enables improved reconstruction of a transcriptome from RNA-seq reads, Nat. Biotechnol. 33 (2015) 290–295.

[23] H. Varet, L. Brillet-Guéguen, J.Y. Coppee, M.A. Dillies, SARTools: a DESeq2- and EdgeR-based R pipeline for comprehensive differential analysis of RNA-Seq data, PLoS ONE 11 (2016) e157022.

[24] T. Wu, E. Hu, S. Xu, M. Chen, P. Guo, Z. Dai, T. Feng, L. Zhou, W. Tang, L. Zhan, X. Fu, S. Liu, X. Bo, G. Yu, ClusterProfiler 4.0: A universal enrichment tool for interpreting omics data, Innovation 2 (2021) 100141.

[25] C. Chen, H. Chen, Y. Zhang, H.R. Thomas, M.H. Frank, Y. He, R. Xia, Tbtools: an integrative toolkit developed for interactive analyses of big biological data, Mol. Plant 13 (2020) 1194–1202.

[26] L. Nayak, D. Panda, G.K. Dash, M.K. Lal, P. Swain, M.J. Baig, A. Kumar, A chloroplast glycolate catabolic pathway bypassing the endogenous photorespiratory cycle enhances photosynthesis, biomass and yield in rice (*Oryza sativa* L.), Plant Sci. 314 (2022) 111103.

[27] C. Peterhansel, C. Blume, S. Offermann, Photorespiratory bypasses: how can they work?, J. Exp. Bot. 64 (2013) 709–715.

[28] D. Leister, Enhancing the light reactions of photosynthesis: strategies, controversies, and perspectives, Mol. Plant 16 (2023) 4–22.

[29] R. Croce, E. Carmo-Silva, Y.B. Cho, M. Ermakova, J. Harbinson, T. Lawson, A.J. McCormick, K.K. Niyogi, D.R. Ort, D. Patel-Tupper, P. Pesaresi, C. Raines, A.P.M. Weber, X.G. Zhu, Perspectives on improving photosynthesis to increase crop yield, Plant Cell 36 (2024) 3944–3973.

[30] Y. Suzuki, T. Miyamoto, R. Yoshizawa, T. Mae, A. Makino, Rubisco content and photosynthesis of leaves at different positions in transgenic rice with an overexpression of *RBCS*, Plant Cell Environ. 32 (2009) 417–427.

[31] A. Bahaji, J. Li, Á.M. Sánchez-López, E. Baroja-Fernández, F.J. Muñoz, M. Ovecka, G. Almagro, M. Montero, I. Ezquer, E. Etxeberria, J. Pozueta-Romero, Starch biosynthesis, its regulation and biotechnological approaches to improve crop yields, Biotechnol. Adv. 32 (2014) 87–106.

[32] L. Huang, H. Tan, C. Zhang, Q. Li, Q. Liu, Starch biosynthesis in cereal endosperms: an updated review over the last decade, Plant Commun. 2 (2021) 100237.

[33] B. Li, A. Huang, L. Wang, S. Wu, Z. Xu, X. Chen, Z. Zhang, X. Peng, Increased sugar content impairs pollen fertility and reduces seed-setting in high-photosynthetic-efficiency rice, Crop J. 12 (2024) 1547–1558.

[34] G. Chen, Y. Li, K. Jin, J. Gao, S. Wu, X. Cui, C. Mao, X. Yin, T. Lu, Z. Zhang, Synthetic photorespiratory bypass improves rice productivity by enhancing photosynthesis and nitrogen uptake, Plant Cell 37 (2025) koaf015.

[35] S.P. Long, X.G. Zhu, S.L. Naidu, D.R. Ort, Can improvement in photosynthesis increase crop yields?, Plant Cell Environ. 29 (2006) 315–330.

[36] R.T. Furbank, W.P. Quick, X.R.R. Sirault, Improving photosynthesis and yield potential in cereal crops by targeted genetic manipulation: Prospects, progress and challenges, Field Crops Res. 182 (2015) 19–29.

[37] A. Garcia, O. Gaju, A.F. Bowerman, S.A. Buck, J.R. Evans, R.T. Furbank, M. Gilliham, A.H. Millar, B.J. Pogson, M.P. Reynolds, Y.L. Ruan, N.L. Taylor, S.D. Tyerman, O.K. Atkin, Enhancing crop yields through improvements in the efficiency of photosynthesis and respiration, New Phytol. 237 (2023) 60–77.

[38] Y. Tao, L. Chiu, J.W. Hoyle, R.A. Dewhirst, C. Richey, K. Rasmussen, J. Du, P. Mellor, J. Kuiper, D. Tucker, A. Crites, G.A. Orr, M.J. Heckert, D. Godinez-Vidal, M.L. Orozco-Cardenas, M.E. Hall, Enhanced photosynthetic efficiency for increased carbon assimilation and woody biomass production in engineered hybrid poplar, Forests 14 (2023) 827.

[39] P.E. López-Calcagno, S. Fisk, K.L. Brown, S.E. Bull, P.F. South, C.A. Raines, Overexpressing the H-protein of the glycine cleavage system increases biomass yield in glasshouse and field-grown transgenic tobacco plants, Plant Biotechnol. J. 17 (2019) 141–151.